IEEE Access
Multidisciplinary | Rapid Review | Open Access Journal

Received 11 January 2025, accepted 17 January 2025, date of publication 20 January 2025, date of current version 29 January 2025.

Digital Object Identifier 10.1109/ACCESS.2025.3532516

RESEARCH ARTICLE

Decentralized Frequency Regulation by Using Novel PID Sliding Mode Structure in Multi-Area Power Systems With Hydropower Turbines

DAO TRONG TRAN[1], ANH-TUAN TRAN[1], VAN VAN HUYNH[1], AND TON DUC DO[2], (Senior Member, IEEE)

[1]Modeling Evolutionary Algorithms Simulation and Artificial Intelligence, Faculty of Electrical and Electronics Engineering, Ton Duc Thang University, Ho Chi Minh City, Vietnam

[2]Department of Robotics and Mechatronics, School of Engineering and Digital Sciences (SEDS), Nazarbayev University, 010000 Astana, Kazakhstan

Corresponding author: Anh-Tuan Tran (trananhtuan1@tdtu.edu.vn)

ABSTRACT This paper introduces a novel sliding mode control (SMC) design utilizing a Proportional-Integral-Derivative (PID) Sliding Surface (SS) for frequency regulation in multi-area electrical power systems (EPSs) with hydropower turbines, accounting for random load conditions, parameter variations, and matched uncertainties. The global system stability of this new approach is mathematically analyzed using Lyapunov theory alongside a novel Linear Matrix Inequality (LMI) technique. A robust strategy is employed through the reaching law method to ensure that frequency deviations converge to zero, even under varying load demands. Despite the presence of parameter variations and random load conditions, the control objectives remain achievable, highlighting the robustness of the proposed method. Moreover, this strategy results in lower overshoot, quicker response times, and reduced chattering effects compared to current traditional SMCs including Proportional-Integral (PI), double PI (DPI), and Proportional-Derivative (PD) sliding surfaces, demonstrating its advantages. Finally, the effectiveness of the suggested scheme is further verified based on three-area EPSs with matched uncertainties, indicating that the proposed scheme achieves stable and robust performance, further confirming its superiority through simulation results.

INDEX TERMS Electrical power system, load frequency control, sliding mode control.

I. INTRODUCTION

In multi-area electrical power systems (EPSs), keeping frequency stability is a critical task to ensure the reliable grid's operation [1], [2]. The EPS frequency reflects the balance between load demand and power generations. Any variation from the nominal frequency can lead to severe operational problems, including equipment malfunction, reduced power quality, and even blackouts. Consequently, load frequency control (LFC) plays a key role in keeping system frequency within allowable limits by dynamically managing generation levels to match fluctuations in demand [3], [4], [5]. Especially for hydropower EPSs, hydropower turbines typically have a more flexible response to frequency changes due to their ability to regulate water flow and adjust power output quickly. While they possess high inertia, which generally slows their initial response, their capability to rapidly adjust the water flow allows for quicker compensation of frequency deviations. In contrast, thermal EPS exhibit slower dynamics due to the inertia of their steam generation processes, requiring additional support systems for effective LFC. The inherent flexibility and ability of hydropower to adjust water flow make it particularly well-suited for LFC compared to other turbine-based systems [6].

Traditional control methods, such as proportional-integral-derivative controllers (PID), have been widely employed for LFC due to their simplicity and ease of implementation [7], [8], [9]. However, these methods struggle to maintain performance in systems characterized by nonlinearity, uncertainties, and external disturbances, especially renewable energy sources (RESs) such as solar and wind power.

The associate editor coordinating the review of this manuscript and approving it for publication was Fabio Mottola.

The introduction of these intermittent sources has increased the complexity of frequency control due to their unpredictable nature. Therefore, to overcome the limitations of traditional PID controllers, integrating modern algorithms has become a crucial trend in both research and practical applications. These hybrid approaches help optimize and improve the PID's performance [10], [11] and modified PID schemes [12], [13], [14]. In [11], the author introduced a groundbreaking 1PD-PI controller optimized by Mountaineering Team-based optimization for LFC in islanded microgrids. The work is applied to various power sources, consists of diesel engine generators, microturbines, fuel cells, RESs, and energy storage systems, evaluating the efficiency, sensitivity, and robustness of the suggested scheme. Although PID control methods are easy to fine-tune through algorithms to improve performance, they still struggle to cope with nonlinearities in the system, which can lead to oscillations and instability under varying operating conditions.

To address this issue, advanced control schemes such as fuzzy logic control (FLC) have been designed [15], [16], [17]. In [16], Kumar et al. designed a new hybrid scheme based on optimization and FLC for LFC of an isolated EPS with non-reheat turbines. The uncertain parameters of the suggested scheme were chosen utilizing the Big Bang-Big Crunch algorithm. A reduced single-area LFC was used to verify the controller's performance in terms of error parameters and transient response. However, its performance depends on the completeness of the fuzzy rule base, and the inference process can be computationally expensive, particularly when dealing with a large number of rules.

Furthermore, deep learning has been employed as a modern approach to controlling load frequency [18], [19], [20]. A multi-agent deep reinforcement learning approach in the continuous action domain for LFC of EPSs was developed in [19]. This approach adaptively and nonlinearly determines an optimal coordinated control scheme for LFC scheme by utilizing decentralized implementation and centralized learning. A three-area EPSs and a fully modeled 39-bus New England system were used under load demand and renewable power changes to assess the suggested controller's robustness. However, this method requires extensive training data, risks overfitting, and its ''black-box'' nature makes it difficult to interpret and adjust.

Another advanced method adopted for LFC is optimal control [21], [22]. In [21], the authors employed an optimal output feedback controller based on full output state control for multi-source EPS LFC, including reheat, hydro, and gas turbines. Generation rate constraints were applied to ensure applicability. Additionally, a hydro EPS LFC operational in Iran's province was employed to depict the suggested approach's effectiveness in a practical case. However, it depends heavily on accurate system models and is less effective for nonlinear systems, with increasing computational demands as system complexity grows.

Model predictive control (MPC) is another robust approach for adjusting load frequency within allowable ranges [23], [24]. In [23], the authors developed an adaptive MPC scheme for EPS LFC integrated with wind, photovoltaic, and thermal power. The proposed approach improves EPS performance and reduces issues related to oscillations due to system parameter variations and load demand changes. However, MPC is computationally intensive and relies on precise system models, complicating real-time implementation in dynamic EPSs.

SMC [25], [26], [27], [28], [29], [30], [31], [32], [33] has gained attention in recent years for its robustness to system uncertainties and disturbances. The major feature of SMC scheme is its ability to drive system states to a predefined sliding surface (SS) and maintain them there, ensuring insensitivity to model variations and external disturbances. The study in [25] presents a quantized SMC for a Markov Jump System-based model for remote area weak grids, addressing and stabilizing system dynamics. A double SMC strategy combining wind turbine pitch control and an adaptive LFC for diesel generators in isolated micro-grids with RESs was proposed in [26]. Study in [27] introduced a non-linear SMC for three-area EPS LFC, addressing uncertainties and disturbances. The controller improves performance, reduces settling time and chattering, and is assessed on the IEEE 39-bus system. In [28], a full-order SMC for LFC, combining terminal and linear methods to eliminate singularities, reduce chattering, and improve response time under various load disturbances. Study in [29] presented a Terminal SMC optimized using the Artificial Bee Colony algorithm for LFC in islanded micro-grids. The method ensures finite-time stability and improved performance in damping frequency oscillations under disturbances. Study in [30] presented a new discrete-time SMC-based full-state feedback control for LFC in a four-area EPSs including thermal and hydropower sources. The proposed scheme for robust LFC was developed using a genetic algorithm, ensuring greater disturbance rejection and avoiding overshoot. However, designing discrete controllers to match continuous-time system behaviors can increase computational overhead. In [31], a backstepping SMC scheme for a two-area thermal linked EPSs under parameter uncertainties and load disturbances was introduced. The suggested controller's effectiveness was assessed by comparing it with second-order SMC, observer-based SMC, and port-Hamiltonian PID controllers. The backstepping SMC method allows for more flexible control design but comes at the cost of increased computational complexity and potential performance degradation in highly dynamic or noisy environments.

A novel decentralized LFC scheme based on integral SMC and PI for multi-area EPSs (MAEPS) under matched and mismatched uncertainties was developed in [32]. Study in [33] developed a double-integral single-phase SMC-based observer for in MAEPS LFC with solar power sources. However, first-order SMCs present the issue of causing a chattering effect, which can potentially harm power equipment and compromise system stability. To overcome this, second-order SMC-based observers and decentralized higher-order SMCs

were designed in [34], [35], and [36], respectively. These methods introduce high design complexity, particularly in handling time-varying parameters, making them challenging to apply in industry. Study in [37] presented a novel PD SMC for controlling system frequency in linked EPSs. The boundedness and reachability of the proposed approach were mathematically verified, and its robustness was compared with other SMC methods. While the controller performed well, under constant disturbances or load changes, PD SMC may result in a persistent deviation from the desired setpoint.

In this paper, we propose a novel SMC strategy based on a PID SS. This control approach is simpler and more effective than conventional SS structures like PI SMC [32], double-PI SMC [33], and PD SMC [37]. The simulation results are compared with existing methods [32], [33], [37] to demonstrate the controller's robustness and reliability. Additionally, in comparison to advanced control techniques such as FLC, deep learning, optimal control, and MPC [15], [18], [22], [24], the proposed PID SMC strategy offers significant advantages in terms of simplicity and computational efficiency. While other methods-based controllers often require high computational resources and detailed system models, the PID-SMC combines robustness to system uncertainties with fast response times, offering a practical and effective solution for LFC in MAEPSs with hydropower turbines.

The paper's key contributions are as follows:

- Development of a novel PID-based SS for SMC tailored to hydropower MAEPSs, offering simplicity and effectiveness compared to conventional SSs like PI SMC [32], DPI SMC [33], and PD SMC [37].
- Establishment of a Lyapunov-based LMI theory specifically designed for rigorous and efficient stability and reachability analysis of the proposed PID-SMC strategy, ensuring robust and reliable performance in hydropower MAEPSs.
- The suggested scheme is compared with existing SMC structures, demonstrating its superior performance in terms of over/under shoot and settling time.
- Simulated results on MAEPSs with hydropower turbines, indicate that the suggested approach is robust and stable against random load fluctuations, parameter variations and matched uncertainties.

The paper's structure is listed as follows: Section II displays the MAEPS scheme. Section III illustrates the proposed PIDSMC approach and problem formulation structure. Section IV depicts the simulated result analysis. Finally, Section V displays the conclusion and recommendation.

II. ANALYSIS DYNAMIC MODEL OF ELECTRICAL POWER SYSTEM

Fig 1 displays a typical control diagram of i^{th} area of MAEPSs with hydropower turbines. The main purpose of LFC in each area must maintain its tie-line power and frequency between neighboring area as a constant. Then, each area of EPS dynamics can be illustrated by different equations as follows:

$$\Delta\dot{f}_i(t) = -\frac{1}{T_{pi}}\Delta f_i(t) + \frac{K_{pi}}{T_{pi}}\Delta P_{mi}(t) - \frac{K_{pi}}{T_{pi}}\Delta P_{di}(t) - \frac{K_{pi}}{2\pi T_{pi}}T_{ij}[\Delta\delta_i(t) - \Delta\delta_j(t)] \quad (1)$$

$$\Delta\dot{P}_{mi}(t) = \frac{2T_{RSi}}{T_{RHi}T_{GHi}R_i}\Delta f_i(t) + (\frac{2}{T_{Wi}} + \frac{2}{T_{RHi}})\Delta P_{vi}(t) - \frac{2}{T_{Wi}}\Delta P_{mi}(t) - \frac{2}{T_{Wi}}\Delta P_{mi}(t) + (\frac{2T_{RSi}}{T_{RHi}T_{GHi}} - \frac{2}{T_{RHi}})\Delta P_{gi}(t) - \frac{2T_{RSi}}{T_{RHi}T_{GHi}}\Delta P_{si}(t) \quad (2)$$

$$\Delta\dot{P}_{vi}(t) = \frac{-T_{RSi}}{T_{RHi}T_{GHi}R_i}\Delta f_i(t) + \frac{-1}{T_{RHi}}\Delta P_{vi}(t) + (\frac{1}{T_{RHi}} - \frac{T_{RSi}}{T_{RHi}T_{GHi}})\Delta P_{gi}(t) + \frac{T_{RSi}}{T_{RHi}T_{GHi}}\Delta P_{si}(t) \quad (3)$$

$$\Delta\dot{P}_{gi}(t) = -\frac{1}{T_{GHi}R_i}\Delta f_i(t) - \frac{1}{T_{GHi}}\Delta P_{gi}(t) + \frac{1}{T_{GHi}}\Delta P_{si}(t) \quad (4)$$

$$\Delta\dot{E}_i(t) = B_iK_{Ii}\Delta f_i(t) + \frac{K_{Ii}}{2\pi}T_{ij}[\Delta\delta_i(t) - \Delta\delta_j(t)] \quad (5)$$

$$\Delta\dot{\delta}_i(t) = 2\pi\,\Delta f_i(t) \quad (6)$$

where $i = 1, .., N$ is areas number in MAEPSs; $\Delta f_i(t)$ is frequency fluctuations; $\Delta P_{mi}(t)$ is power output deviations of hydraulic, $\Delta P_{vi}(t)$ is power output fluctuations of governor; $\Delta P_{gi}(t)$ is power output fluctuations of governor, $\Delta E_i(t)$ is area control error fluctuations, $\Delta\delta_i(t)$ is the rotor angle fluctuations, and $\Delta P_{si}(t)$ is control signal of proposed sliding mode controller (SMCer); K_{pi} is EPS operation factor, T_{pi} is time constants of EPSs; T_{GHi}, T_{RSi} and T_{RHi} are hydro turbine speed governor in main servo, reset time, transient, respectively; T_{Wi} is nominal starting time of water in penstock; R_i is governor speed regulation parameters; B_i is frequency bias factors.

The EPS model is presented in Figure 1 which can be revised in following state-space equation below

$$\dot{x}_i(t) = A_ix_i(t) + B_iu_i(t) + C_{ij}x_j(t) + D_i\Theta_i(t) \quad (7)$$

where

$$x_i(t) = \left[\Delta f_i(t)\ \Delta P_{mi}(t)\ \Delta P_{vi}(t)\ \Delta P_{hi}(t)\ \Delta E_i(t)\ \Delta\delta_i(t)\right]^T$$

From these equations, we can design the matrices A_i, B_i, C_{ij}, D_i for MAEPSsas follows: as shown in the equation at the bottom of the next page.

In a real-world MAEPSs, obtaining exact measurements of parameter values is not feasible. Therefore, almost parameters are either estimated or approximate. Moreover, considering the time delay factor, the dynamic model in equation (18) is further modified as:

$$\dot{x}_i(t) = \bar{A}_ix_i(t) + \bar{B}_iu_i(t) + \bar{C}_{ij}x_j(t) + \bar{D}_i\Theta_i(t)$$

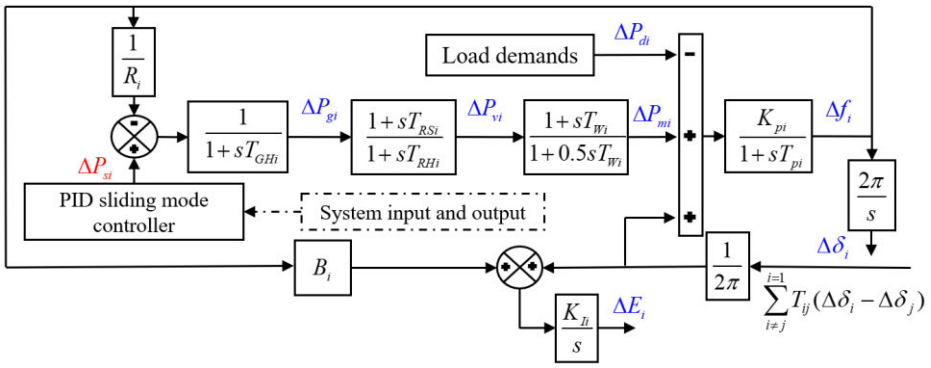

FIGURE 1. The i^{th} area of linked EPS dynamic with proposed controller.

$$= A_i x_i(t) + B_i u_i(t) + C_{ij} x_j(t) + \Omega_i(t) \tag{8}$$

where $\bar{A}_i = A_i + \Delta A_i$, $\bar{B}_i = B_i + \Delta B_i$, $\bar{C}_i = C_i + \Delta C_i$, $\bar{D}_i = D_i + \Delta D_i$ and the unknown matrices ΔA_i, ΔB_i, ΔC_i and ΔD_i are system fluctuations, the matrices A_i, B_i, C_i and D_i are the standard values; $w_i(t)$ is considered the total disturbances which can be predicted and can rewritten it below:

$$\Omega_i(t) = \Delta A_i x_i(t) + \Delta B_i u_i(t) + \Delta C_{ij} x_j(t) + \bar{D}_i \psi_i(t)$$

III. NOVEL SLIDING MODE DESIGN

SMC has been established as a robust control method, particularly effective for systems with incomplete modeling and nonlinear dynamics [38], [39]. In [38], SMC is applied to uncertain nonlinear systems, demonstrating its ability to handle systems with incomplete models by compensating for structural uncertainties and external disturbances. Similarly, in [39], SMC is integrated into a robust fuzzy design for nonlinear uncertain stochastic systems. However, traditional SMC approaches face a critical challenge in the form of high-frequency oscillations, commonly referred to as the chattering problem, caused by rapid switching control near the sliding surface. To address this issue, this article introduces a novel SMC design that incorporates a PID-based SS for MAEPSs. The proposed SMC enhances the transient

$$A_i = \begin{bmatrix} -\frac{1}{T_{pi}} & \frac{K_{pi}}{T_{pi}} & 0 & 0 & 0 & -\frac{K_{pi}}{2\pi T_{pi}} T_{ij} \\ \frac{2T_{RSi}}{T_{RHi}T_{GHi}R_i} & -\frac{2}{T_{Wi}} & (\frac{2}{T_{Wi}} + \frac{2}{T_{RHi}}) & (\frac{2T_{RSi}}{T_{RHi}T_{GHi}} - \frac{2}{T_{RHi}}) & 0 & 0 \\ \frac{-T_{RSi}}{T_{RHi}T_{GHi}R_i} & 0 & \frac{-1}{T_{RHi}} & (\frac{1}{T_{RHi}} - \frac{T_{RSi}}{T_{RHi}T_{GHi}}) & 0 & 0 \\ -\frac{1}{T_{GHi}R_i} & 0 & 0 & -\frac{1}{T_{GHi}} & 0 & 0 \\ B_i K_{Ii} & 0 & 0 & 0 & 0 & \frac{K_{Ii}}{2\pi} T_{ij} \\ 2\pi & 0 & 0 & 0 & 0 & 0 \end{bmatrix}$$

$$B_i = \begin{bmatrix} 0 & -\frac{2T_{RSi}}{T_{RHi}T_{GHi}} & \frac{T_{RSi}}{T_{RHi}T_{GHi}} & \frac{1}{T_{GHi}} & 0 & 0 \end{bmatrix}^T$$

$$C_{ij} = \begin{bmatrix} 0 & 0 & 0 & 0 & 0 & -\frac{K_{pi}}{2\pi T_{pi}} T_{ij} \\ 0 & 0 & 0 & 0 & 0 & 0 \\ 0 & 0 & 0 & 0 & 0 & 0 \\ 0 & 0 & 0 & 0 & 0 & 0 \\ 0 & 0 & 0 & 0 & 0 & \frac{K_{Ii}}{2\pi} T_{ij} \\ 0 & 0 & 0 & 0 & 0 & 0 \end{bmatrix}$$

$$D_i = \begin{bmatrix} -\frac{K_{pi}}{T_{pi}} & 0 & 0 & 0 & 0 & 0 \end{bmatrix}^T$$

performance of the closed-loop system while effectively mitigating oscillations and minimizing chattering.

Previous studies have explored various SMC designs to address control challenges in MAEPSs. In [37], the proposed PD-SMC method demonstrated quick response to transient disturbances due to its PD-SMC structure. However, it exhibited limitations in eliminating steady-state error, resulting in residual inaccuracies that affect long-term stability. [32] introduced PI-SMC, which improved steady-state error reduction by adding integral action, but this came at the expense of slower response times, making the controller less effective under rapidly changing conditions. Building upon these approaches, [33] proposed a double PI- SMCer, which further minimized steady-state error and enhanced robustness against sustained disturbances by incorporating dual integral terms. Nonetheless, this method required complex tuning and tended to exhibit slower response times and potential overshoot, particularly in dynamic environments. To address these limitations, this paper proposes a PID-SMCer that integrates proportional-integral-derivative terms, leveraging the advantages of each previous method. The addition of the derivative term enhances transient response, while the integral components maintain steady-state accuracy, providing a well-rounded, robust solution suitable for systems with parameter uncertainties and variable disturbances. This combined approach achieves superior balance in control performance, minimizing both transient and steady-state errors while maintaining high adaptability across diverse operating conditions.

A. NOVEL PID SS DESIGN

It is difficult to calculate exactly for any system model because almost realistic systems are non-linear. There is a certain difference in real and modelled systems during the operating process because *of* plant variations. SMC technique is known as a robust control method. By applying a designed control law, the system trajectory will be driven to a designed SS with any initial condition and keep it thereafter. Then, we introduce the new PID-SS for the MAEPSs

$$\sigma_i[x_i(t)] = S_i x_i(t) + S_i \int_0^t x_i(\tau) d\tau + S_i \dot{x}_i(t) \tag{9}$$

where S_i are the sliding matrices and S_i is designed to secure that matrix $S_i B_i$ is invertible and matrix.

Differentiate $\sigma_i[x_i(t)]$ in Eq. (9) following time and combined with Eq. (8), we have

$$\dot{\sigma}_i[x_i(t)] = S_i A_i x_i(t) + S_i B_i u_i(t) + S_i C_{ij} x_j(t) + S_i N_i(x_i, t) + S_i \dot{x}_i(t) + S_i \ddot{x}_i(t) \tag{10}$$

Establishing $\dot{\sigma}_i[x_i(t)] = \sigma_i[x_i(t)] = 0$, then controller is designed as

$$u_i(t) = -(S_i B_i)^{-1}\{(A_i + I) S_i x_i(t) + S_i C_{ij} x_j(t) + S_i \ddot{x}_i(t) + \delta_i \operatorname{sgn}\{\sigma_i[x_i(t)]\}\} \tag{11}$$

Then substituting $u_i(t)$ in Eq. (11) into the MAEPSs in Eq. (8), we achieve

$$\ddot{x}_i(t) = -\dot{x}_i(t) - [I - B_i(S_i B_i)^{-1} S_i] C_{ij} x_j(t) - S_i x_i(t) - [I - B_i(S_i B_i)^{-1} S_i] N_i(x_i, t) \tag{12}$$

First supporting, by assuming that

$$\hat{x}_i(t) = \dot{x}_i(t) \tag{13}$$

where $\hat{x}_i(t)$ is the first newly transferred system variable.

Then, Eq. (12) become

$$\dot{\hat{x}}_i(t) = -\hat{x}_i(t) - [I - B_i(S_i B_i)^{-1} S_i] C_{ij} \int_0^t \hat{x}_j(\tau) d\tau - S_i \int_0^t \hat{x}_i(\tau) d\tau - [I - B_i(S_i B_i)^{-1} S_i] N_i(x_i, t) \tag{14}$$

Second supporting, by assuming that

$$m_i(t) = \int_0^t \hat{x}_i(\tau) d\tau; \quad n_i(t) = \hat{z}_i(t) \tag{15}$$

and

$$\dot{m}_i(t) = \hat{x}_i(t) = n_i(t) \tag{16}$$

where $m_i(t)$ and $n_i(t)$ are the second newly transferred system variables.

Substituting Eqs. (15) and (16) into Eq. (14), then it can be rewritten below

$$\dot{n}_i(t) = -n_i(t) - [I - B_i(S_i B_i)^{-1} S_i] C_{ij} m_j(t) - S_i m_i(t) - (S_i)^{-1} [I - B_i(S_i B_i)^{-1} S_i] N_i(x_i, t) \tag{17}$$

The sliding equation can be revised below

$$\dot{d}_i(t) = \bar{A}_i d_i(t) + \bar{C}_i d_j(t) + \bar{D}_i N_i(x_i, t) \tag{18}$$

where

$$d_i(t) = \begin{bmatrix} n_i(t) \\ m_i(t) \end{bmatrix}; \quad \bar{A}_i = \begin{bmatrix} -I & S_i \\ 0 & I \end{bmatrix};$$
$$\bar{C}_i = \begin{bmatrix} 0 & [I - B_i(S_i B_i)^{-1} S_i] C_{ij} \\ 0 & 0 \end{bmatrix};$$
$$\bar{D}_i = \begin{bmatrix} [I - B_i(S_i B_i)^{-1} S_i] \\ 0 \end{bmatrix}$$

B. THEORETICAL PROVE OF GLOBAL SYSTEM ON NEW SLIDING SURFACE

It is important to demonstrate the global stabilization of the MAEPSs. In this work, theoretical analysis of differential systems is conducted using Lyapunov theory. Additionally, several lemmas are also employed and LMI theorem adopted to support the mentioned stabilization proves.

Lemma 1 [35]: Let P and Q are realistic matrices with suitable dimension then, for any scalar $\tau > 0$, the following matrix inequality achieve

$$P^{\mathbf{T}} Q + Q^{\mathbf{T}} P \leqslant \tau P^{\mathbf{T}} P + \tau^{-1} Q^{\mathbf{T}} Q.$$

Lemma 2 [35]: Matrix:

$$\begin{bmatrix} P(\bar{x}) & R(\bar{x}) \\ R^T(\bar{x}) & Q(\bar{x}) \end{bmatrix} > 0$$

where $P(\bar{x}) = P^T(\bar{x})$, $Q(\bar{x}) = Q^T(\bar{x})$ and $R(\bar{x})$ which depends on $\bar{x}$. Therefore, $Q(\bar{x}) > 0$ and $P(\bar{x}) - R(\bar{x})Q^{-1}(\bar{x})R^T(\bar{x}) > 0$.

Theorem 1: The sliding motion described in (12) is considered asymptotically stable if there exists a symmetric positive definite matrix H_i, along with positive scalars μ_{j1}, μ_{i1}, and μ_{i2} ($i = 1, 2, \ldots, N$). Then following LMI as

$$\begin{bmatrix} \bar{A}_i^T H_i + H_i \bar{A}_i & \bar{C}_i^T & H_i & \bar{D}_i^T H_i \\ \bar{C}_i & \mu_{j1} & 0 & 0 \\ H_i & 0 & \mu_{i1}^{-1} & 0 \\ H_i \bar{D}_i & 0 & 0 & \mu_{i2} \end{bmatrix} < 0 \tag{19}$$

Proof 2: To demonstrate the sliding motion's stability (12), we set the Lyapunov form as

$$V_1(t) = \sum_{i=1}^{N} \left[d_i^T(t) H_i d_i(t) \right] \tag{20}$$

where $H_i > 0$ satisfied Eq. (19).

Then, taking the derivative of $V_1(t)$:

$$\dot{V}_1(t) = \sum_{i=1}^{N} \left[\dot{d}_i^T(t) H_i d_i(t) + d_i^T(t) H_i \dot{d}_i(t) \right] \tag{21}$$

and using Eq. (18), we achieve:

$$\dot{V}_1(t) = \sum_{i=1}^{N} \left\{ \begin{array}{c} \bar{A}_i^T d_i^T(t) H_i d_i(t) + d_i^T(t) H_i \bar{A}_i d_i(t) \\ + \bar{C}_i^T d_j^T(t) H_i d_i(t) + d_i^T(t) H_i \bar{C}_i d_j(t) \\ + \bar{D}_i^T N_i^T(x_i, t) H_i d_i(t) + d_i^T(t) H_i \bar{D}_i N_i(x_i, t) \end{array} \right\} \tag{22}$$

Employing Lemma 1 to equation (22), yields

$$\dot{V}_1(t) < \sum_{i=1}^{N} \left\{ \begin{array}{c} d_i^T(t)[\bar{A}_i^T H_i + H_i \bar{A}_i] d_i(t) \\ + \mu_{i1} d_i^T(t) \bar{C}_i^T \bar{C}_i d_j(t) + \mu_{i1}^{-1} d_i^T(t) H_i H_i d_i(t) \\ + \mu_{i2} d_i^T(t) \bar{D}_i^T H_i H_i \bar{D}_i d_i(t) + \mu_{i2}^{-1} N_i^T(x_i, t) N_i(x_i, t) \end{array} \right\} \tag{23}$$

Since

$$\sum_{i=1}^{N} \sum_{\substack{j=1 \\ i \neq j}}^{N} \mu_{i1} d_j^T(t) \bar{C}_i^T \bar{C}_i d_j(t) = \sum_{j=1}^{N} \sum_{\substack{i=1 \\ j \neq i}}^{N} \mu_{j1} d_i^T(t) \bar{C}_i^T \bar{C}_i d_i(t)$$

Then, applying Assumption 1, Eq. (23) can be defined as:

$$\dot{V}_1(t) < \sum_{i=1}^{N} \left\{ \begin{array}{c} d_i^T(t)[\bar{A}_i^T H_i + H_i \bar{A}_i + \mu_{j1} \bar{C}_i^T \bar{C}_i + \mu_{i1}^{-1} H_i H_i \\ + \mu_{i2} \bar{D}_i^T H_i H_i \bar{D}_i] d_i(t) + \mu_{i2}^{-1} \varepsilon_i^T \varepsilon_i \end{array} \right\} \tag{24}$$

In addition, by using Lemma 2, LMI (24) is equivalent to this inequality

$$-\Phi_i = \bar{A}_i^T H_i + H_i \bar{A}_i + \mu_{j1} \bar{C}_i^T \bar{C}_i + \mu_{i1}^{-1} H_i H_i + \mu_{i2} \bar{D}_i^T H_i H_i \bar{D}_i < 0 \tag{25}$$

From equations (29) and (30), we achieve

$$\dot{V}_1(t) \leqslant \{ -\lambda_{\min}[(-\Phi_i)\|d_i(t)\|^2] + \delta_i \} \tag{26}$$

where the value $\delta_i = \mu_{i2}^{-1} \varepsilon_i^T \varepsilon_i$ and the eigenvalues of $\lambda_{\min}(-\Phi_i) > 0$. Therefore, $\dot{V}_1(t) < 0$ is achieved with $\|d_i(t)\| > \sqrt{\frac{\delta_i}{\lambda_{\min}(\Phi_i)}}$. Thus, the MAEPSs' sliding motion (8) is asymptotically stable.

Additionally, we demonstrate theoretically the system states' reachability to the PID-SS. We assumed that $d_i(t) > 0$ little above the equilibrium part at the surface, then the Lyapunov form is set below

$$V_2(t) = \frac{1}{2} \sigma_i[x_i(t)] \tag{27}$$

We take the derivative of Eq. (27) based on time, we have

$$\dot{V}_2(t) = \sigma_i[x_i(t)]^T \dot{\sigma}_i[x_i(t)] \tag{28}$$

Substituting Eq. (10) into Eq. (28) then it becomes

$$\begin{aligned} \dot{V}_2(t) = \sigma_i[x_i(t)]^T \{ & S_i A_i x_i(t) + S_i B_i u_i(t) + S_i C_{ij} z_j(t) \\ & + S_i N_i(x_i, t) + S_i x_i(t) + S_i \ddot{x}_i(t) \} \end{aligned} \tag{29}$$

Using the controller in Eq. (11), then

$$\dot{V}_2(t) = -\delta_i \, \|\sigma_i[x_i(t)]\| \tag{30}$$

Thus, Eq. (30) shows that $\dot{V}_2(t) < 0$ which demonstrates the system states' reachability to the PID-SS.

IV. SIMULATED RESULTS

In this section, the simulated results are performed and compared with other previous methods in [32], [33], and [37]. Accordingly, three different scenarios are conducted based on isolate EPSs and three-area linked EPSs with hydropower turbines. Then, nominal parameters for MAEPSs with hydropower turbines are assumed to be the same value with studies [40], [41], presented as follows:

The EPS model: $K_{pi} = 120$; $T_{pi} = 20$; $B_i = 0.425$; $T_{ij} = 0.0342 puMW/rad$; $R_i = 2.4$;

The hydropower turbines: $T_{Wi} = 0.3s$; $T_{RSi} = 5s$; $T_{RHi} = 28.75s$; $T_{GHi} = 0.3s$.

where $i = 1, 2, 3, \ldots, N$ represents the area numbers of MAEPSs.

A. ISOLATED EPS WITH HYDROPOWER TURBINE UNDER STEP LOAD DEMAND

In this case, three SMC structures are simulated at the same condition and configuration in comparison with proposed PID SMC including PI [32], double PI (DPI) [33] and PD [37] SS presented below

PI-SMC: $\sigma_i[x_i(t)] = S_i x_i(t) + S_i \int_0^t x_i(\tau) d\tau$

DPI-SMC: $\sigma_i[x_i(t)] = S_i x_i(t) + S_i \int_0^t x_i(\tau) d\tau + S_i \int_0^t \int_0^t x_i(\tau) d\tau$

TABLE 1. Frequency deviation by four control approach.

Methods	Max (Under/overshoot)	Settling time
Proposed SMC	-0.02425	3s
PD-SMC	-0.02648	11s
PI-SMC	-0.03429	9s
DPI-SMC	-0.03501	11s

PD-SMC: $\sigma_i[x_i(t)] = S_i x_i(t) + S_i \dot{x}_i(t)$

The parameters of matrix S_i can be gained as $[\ -0.52\ \ -0.34\ \ -0.42\ 42.7\ \ -27.92\ 1.72\ ] \times 10^3$ according to the Eq. (9). For power factor in control signal in Eq. (11), the desired value is chosen as $\delta_i = 0.15$. These parameters are chosen to have consistent values across all methods to facilitate comparison.

The external step load change is set 0.015 $p.u$ at $t = 1\ s$. The simulation results in Figs 2 and 3 illustrate that all tested control methods, including proposed scheme, PD, PI, and double PI SMCs, successfully meet the control objectives under identical conditions and configurations. Table 1 provides a detailed comparison of frequency error including defining time and undershoot, for each controller under these conditions.

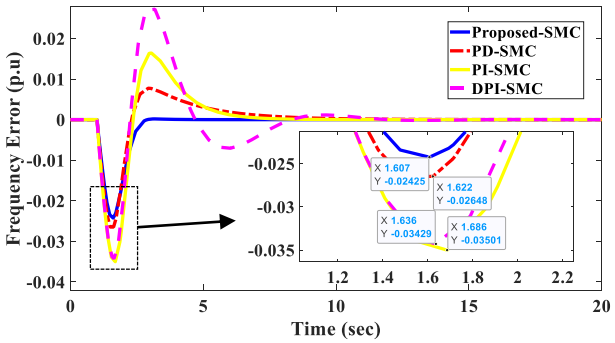

FIGURE 2. EPS frequency errors by four methods under case A.

The data in Table 1 make it evident that the suggested PID-SMC outperforms the other control methods, showcasing both faster response times and superior frequency stabilization. Notably, the frequency error converges to zero more efficiently with the PID-SMCer, achieving a quicker steady-state with minimal undershoot. This enhanced response highlights the advantages of integrating PID structure within an SMC method, which effectively combines rapid transient response with robust steady-state accuracy.

Remark: In this case, the 1.5% step load change results in a 0.03 p.u. frequency deviations, which is significant enough to potentially trigger an under-frequency relay in many EPSs. This highlights a limitation of the LFC approach, as such frequency deviations may activate protective actions like under-frequency load shedding or the disconnection of critical loads. While the proposed LFC method is effective for smaller perturbations, it may require further enhancement to handle larger disturbances or prevent the activation of protective relays in practical systems. Future work could investigate supplementary control strategies to address these challenges.

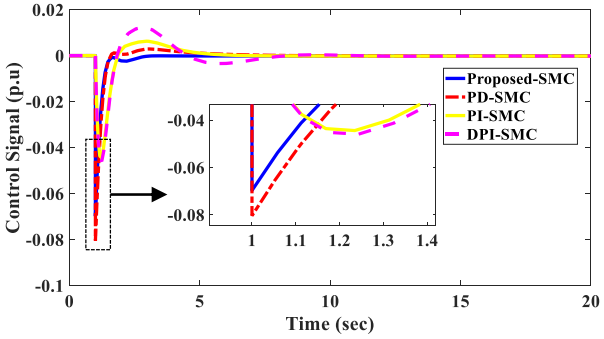

FIGURE 3. Control signals by four methods under case A.

TABLE 2. The parameter variations in two-area linked EPSs.

Parameter		Nominal Values	Variation Range [%]	New Values
Case 1	T_{pi}	20	+25	25
	T_{GHi}	0.3	-25	0.225
	R_i	2.4	-25	1.8
Case 2	T_{pi}	20	+50	30
	T_{GHi}	0.3	-50	0.15
	R_i	2.4	-50	1.2
Case 3	T_{pi}	20	+50	30
	T_{GHi}	0.3	+25	0.375
	R_i	2.4	+50	3.6

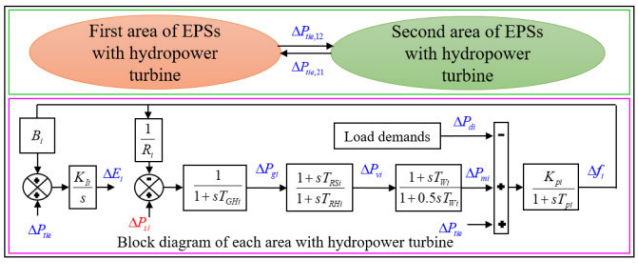

FIGURE 4. Block diagram of two-area linked EPSs.

B. TWO-AREA LINKED EPS WITH HYDROPOWER TURBINES UNDER PARAMETER UNCERTAINTIES AND RANDOM LOAD DEMANDS

In this section, two-area linked EPS model with hydropower turbines is considered as Fig 4. Then, the proposed scheme is verified in the model under conditions of parameter uncertainties and random load demands displayed in Fig 5 is employed to further test the suggested approach.

To thoroughly evaluate the effectiveness of the suggested approach, three scenarios with parameter uncertainties (T_{pi}; T_{GHi}; R_i), as detailed in Table 2, are introduced to

validate its reliability and robustness. These cases involve non-linear variations in parameters associated with the MAEPSs. We can evaluate how well the control method adapts to non-linear behaviors by applying these uncertainties. The performance results will demonstrate whether the suggested control approach maintains stable frequency regulation and quick response under varying conditions, thereby highlighting its suitability for practical applications where parameter fluctuations are common.

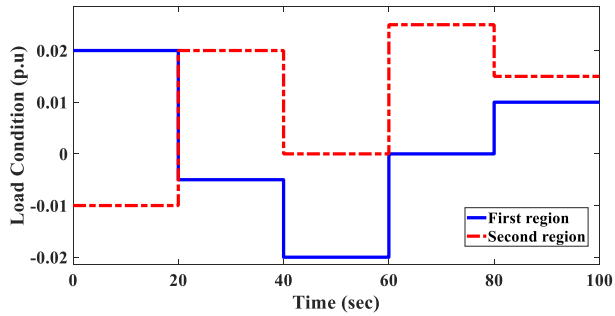

FIGURE 5. Variable load conditions.

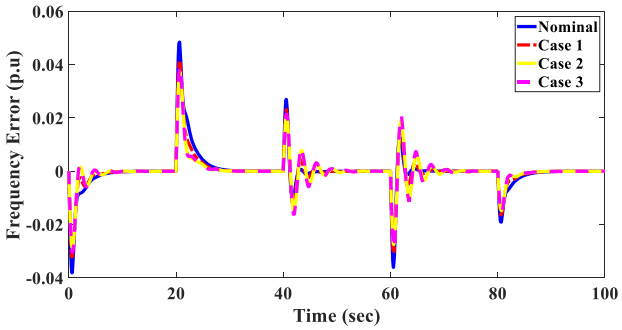

FIGURE 6. EPS frequency errors of the 1^{st} region under case B.

The frequency error depicted in Figs. 6 and 7 illustrates that the suggested controller decreases effectively fluctuations, swiftly returning the frequency to its desired value despite uncertainties in parameters and random load variations. The minimal steady-state error and rapid convergence to zero further highlight the controller's stability and robust frequency regulation.

In Figs. 8, the tie-line power error demonstrates the suggested controller's capability to maintain a balance in power exchange between the two areas. Lastly, the control signals generated by the proposed controller are presented in Figs. 9 and 10.

C. THREE-AREA LINKED EPSS WITH HYDROPOWER TURBINES UNDER MATCHING UNCERTAINTIES

To further verify the suggested PID SMC scheme's robustness, the same matched system uncertainties are set with [33] for three-area linked EPSs with hydropower turbines as displayed in Fig 11 with the element of each area being the same as the previous second case. Then, these uncertainties

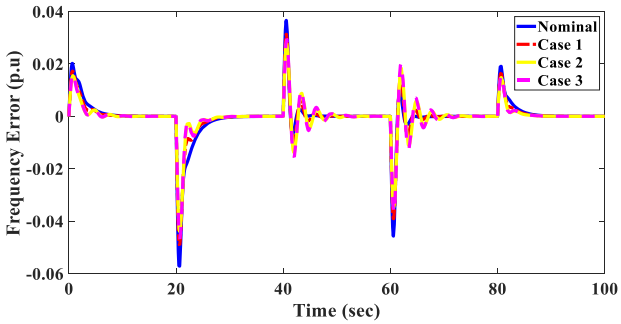

FIGURE 7. EPS frequency errors of the 2^{nd} region under case B.

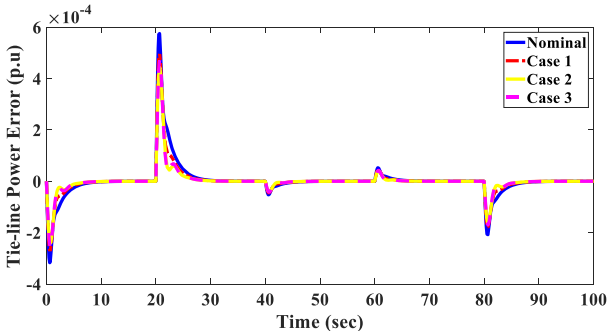

FIGURE 8. EPS tie-line power errors under case B.

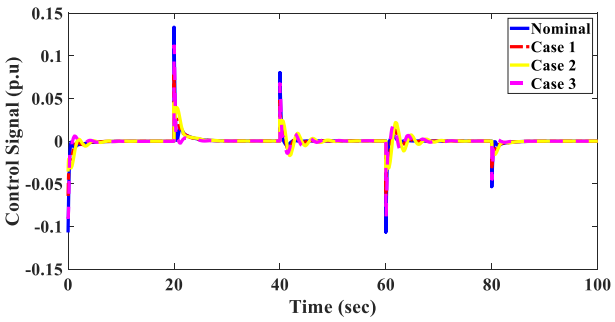

FIGURE 9. Control signals of 1^{st} region under case B.

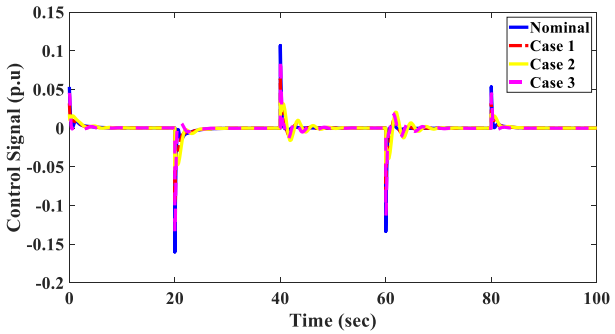

FIGURE 10. Control signals of 2^{nd} region under case B.

are expressed using cosine functions centered around the standard values, as shown below: as shown in the equation at the bottom of page 11.

The step load demands in this case are set respectively as $0.01p.u$, $0.015p.u$, and $0.02p.u$ at $t = 1s$ in area 1, 2 and 3. The simulated results indicate that the robust and resilient

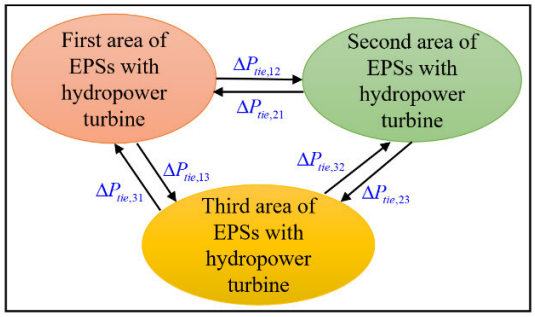

FIGURE 11. Three-area linked EPSs with hydropower turbines.

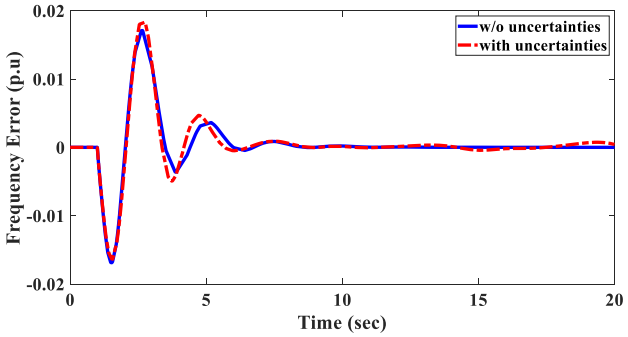

FIGURE 12. EPS frequency errors in 1^{st} region.

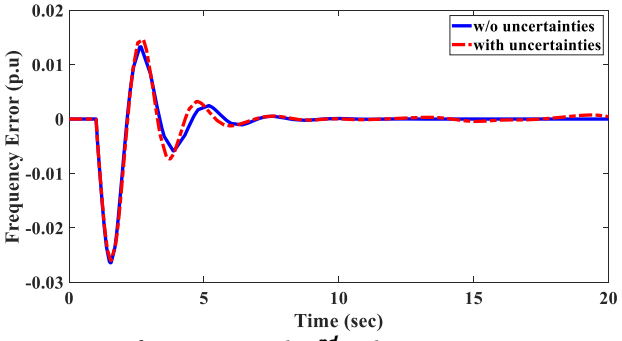

FIGURE 13. EPS frequency errors in 2^{nd} region.

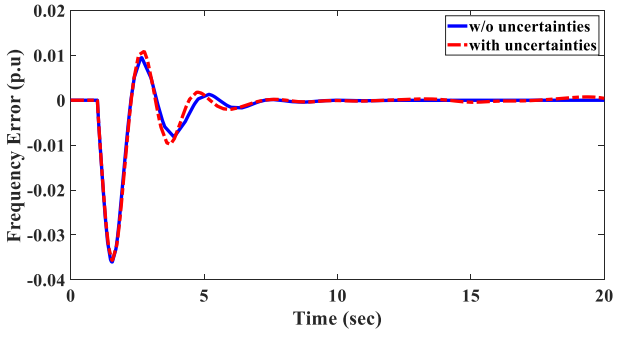

FIGURE 14. EPS frequency errors in 3^{rd} region.

PID SMCer under the influence of matched uncertainties demonstrates that this method effectively handles within the system. These uncertainties, modeled as cosine functions around the standard values of the three-area EPSs with hydropower turbines, serve as a realistic test of the controller's adaptability and robustness.

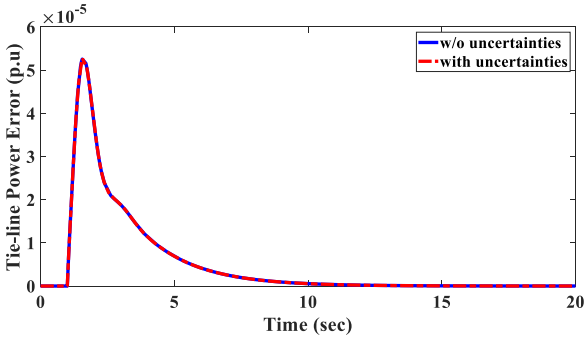

FIGURE 15. EPS tie-line power errors in 1^{st} region.

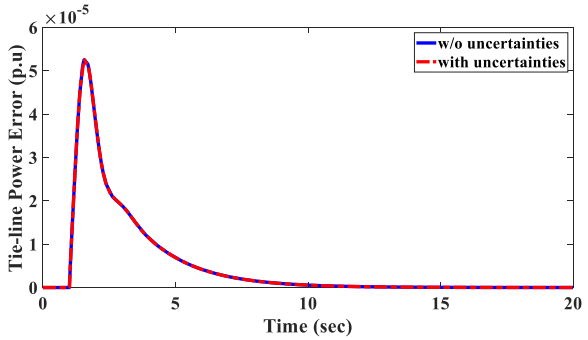

FIGURE 16. EPS tie-line power errors in 2^{nd} region.

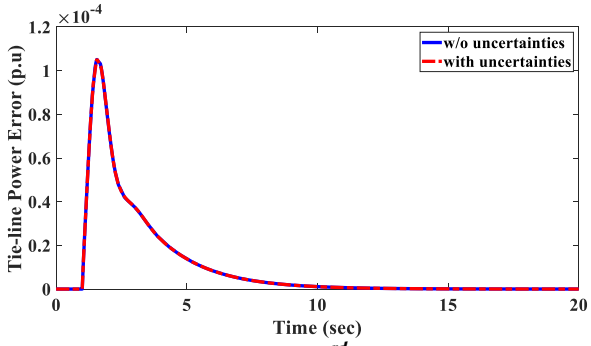

FIGURE 17. EPS tie-line power errors in 3^{rd} region.

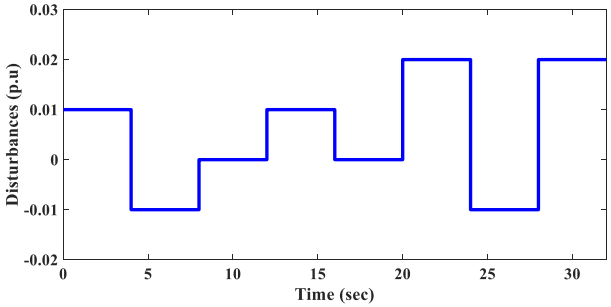

FIGURE 18. Random load demands.

The results displayed from Figs 12 to 17, including tie-line power and frequency errors, indicate that the PID SMCer can quickly and accurately adjust frequency and power variables. This rapid stabilization of the system following disturbances

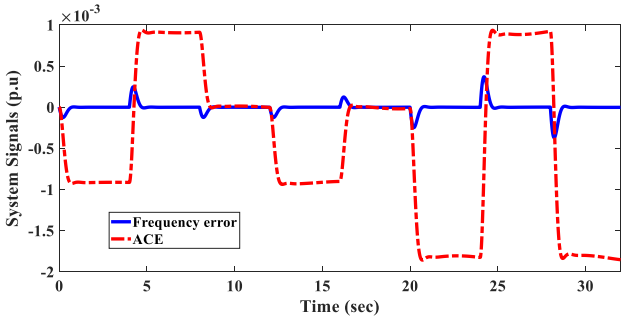

FIGURE 19. System signals of isolated EPS with the proposed controller.

highlights the controller's resilience and stable performance not only under normal conditions but also in the presence of known uncertainties.

Notably, the PID SMC design shows a strong capacity to minimize frequency and power errors even in scenarios with matched uncertainties. The cosine function-based uncertainty representation reflects realistic conditions, validating the controller's robustness and stability. As a result, the PID SMCer can ensure EPS stability while delivering high performance under realistic operational conditions with continuously fluctuating loads.

Finally, the analysis confirms that the PID SMC is a highly effective solution for frequency and power control in MAEPSs with hydropower turbines, particularly in systems prone to matched uncertainties.

D. ISOLATED THERMAL EPS WITH NON-REHEAT TURBINE UNDER RANDOM LOAD DEMANDS

In the final case, an isolated thermal EPS with non-reheat turbine [42] subjected to random load demands is considered. The focus is to examine the suggested strategy's performance. The random load demands displayed in Fig 18 and system parameters are set the same value of study in [42] for comparison. This comparison aims to highlight the relative strengths of the proposed controller, particularly its simplicity and robustness while assessing its effectiveness in terms of settling time, overshoot, and stability under stochastic disturbances.

The random load demands displayed in Fig 18 and system parameters are set the same value of study in [42] for comparison. This comparison aims to highlight the relative strengths of the proposed controller, particularly its simplicity and robustness while assessing its effectiveness in terms of settling time, overshoot, and stability under stochastic disturbances.

Fig 19 depicts the main findings including frequency errors and ACE signal of isolated EPS with the suggested controller. The simulated results from this case are also employed to compare the proposed method against the Deep Reinforcement Learning (DRL) approach in [40] as Table 3. This comparison aims to highlight the relative strengths of the proposed controller, particularly its simplicity and robustness while assessing its effectiveness in terms of settling time, overshoot, and stability under random disturbances.

TABLE 3. Frequency errors of isolated EPSs.

Methods	Max (Under/overshoot)	Settling time
Proposed SMC	-3.7×10^{-4}	1.2s
DRL [40]	-0.0266	2.4s

E. DISCUSSION

The proposed PID SMC scheme has proved significant robustness and broad applicability through detailed testing on isolated, two-area, and three-area EPSs under various conditions. These tests included step and random load disturbances, parameter variations, and matched uncertainties, common challenges encountered in real-world EPS operations. The results indicate that the PID SMCer not only maintains a fast response time but also effectively minimizes steady-state errors, even when the system faces significant fluctuations and non-linearities.

Notably, the controller exhibits flexible adaptability to changes in operating conditions and maintains EPS stability despite parameter uncertainties. The exceptional resilience of the PID SMC ensures that the system remains efficient under unexpected disturbances, preserving frequency stability and regulating tie-line power flow between areas.

These strengths make PID SMC an ideal choice for complex and modern EPSs, where high stability, precision, and rapid response to unforeseen situations are crucial. With its ability to meet diverse requirements and sustain stable performance in continuously changing environments, the PID SMCer demonstrates a high potential for practical application in EPSs with significant complexity and uncertainty.

V. CONCLUSION

This paper introduces a novel SMC strategy using a PID SS to enhance frequency regulation in MAEPSs with hydropower turbines. Designed to address challenges posed by random load fluctuations, parameter variations, and matched uncertainties, the proposed PID SS-based SMC approach offers a resilient and efficient solution for load frequency control. The theoretical analysis, verified by Lyapunov stability and novel LMI techniques, confirms that the PID-SS-based SMC ensures global system stability, while the reaching law method enables frequency deviations to converge to zero under variable load demands. The simulation results, conducted on three types of EPS models including isolated, two-area, and three-area, demonstrate that the proposed approach achieves quicker settling times, reduced overshoot, and minimal chattering effects in comparison to conventional SMC, including PI, double PI, and PD SS methods. This reinforces the robustness and reliability of the PID SS-based SMC design in maintaining system stability even under challenging operating conditions. Future research could further

explore the integration of RESs and consider the use of multiple energy sources to compare the effectiveness and create a more comprehensive system model. Additionally, testing the controller's effectiveness under more complex disturbance scenarios would help enhance its industrial applicability.

$$\Delta A_i = \begin{bmatrix} 0 & 0 & 0 & 0 & 0 & 0 \\ 0 & 0 & 0 & 0 & 0 & 0 \\ 0 & 0 & 0 & 0 & 0 & 0 \\ -2.26\cos(t) & 2\cos(t) & 0 & -2.604\cos(t) & 3\cos(t) & 0 \\ 0 & 0 & 0 & 0 & 0 & 0 \\ 0 & 0 & 0 & 0 & 0 & 0 \end{bmatrix}$$

$$A_i = \begin{bmatrix} -0.040 & 4.800 & 0 & 0 & 0 & -0.026 \\ 0.859 & -6.667 & 6.736 & 1.476 & 0 & 0 \\ -0.171 & 0 & -0.035 & -4.410 & 0 & 0 \\ -2.469 & 0 & 0 & -4.444 & 0 & 0 \\ 0.425 & 0 & 0 & 0 & 0 & 0.005 \\ 6.283 & 0 & 0 & 0 & 0 & 0 \end{bmatrix}$$

$$B_i = [0 \quad -1.546 \quad 0.773 \quad 4.444 \quad 0 \quad 0]^T;$$

$$C_{ij} = \begin{bmatrix} 0 & 0 & 0 & 0 & 0 & -0.026 \\ 0 & 0 & 0 & 0 & 0 & 0 \\ 0 & 0 & 0 & 0 & 0 & 0 \\ 0 & 0 & 0 & 0 & 0 & 0 \\ 0 & 0 & 0 & 0 & 0 & 0.0054 \\ 0 & 0 & 0 & 0 & 0 & 0 \end{bmatrix};$$

$$H_i^1 = \begin{bmatrix} -2\times10^{-10} & 2\times10^{-13} & 9\times10^{-14} & -2\times10^{-13} & -8\times10^{-13} & -5\times10^{-13} \\ 2\times10^{-13} & -7\times10^{-2} & -4\times10^{-2} & -2\times10^{-2} & -1\times10^{-4} & 9\times10^{-6} \\ 9\times10^{-14} & -4\times10^{-3} & -7\times10^{-2} & 1\times10^{-2} & -4\times10^{-5} & 3\times10^{-6} \\ -2\times10^{-13} & -2\times10^{-2} & 1\times10^{-2} & -1\times10^{-2} & 2\times10^{-4} & -1\times10^{-5} \\ -8\times10^{-13} & -1\times10^{-4} & -5\times10^{-5} & 2\times10^{-4} & -8\times10^{-2} & 3\times10^{-4} \\ -5\times10^{-13} & 9\times10^{-6} & 3\times10^{-6} & -1\times10^{-5} & 3\times10^{-4} & -8\times10^{-2} \\ 5\times10^{-8} & 2\times10^{-12} & 1\times10^{-12} & -3\times10^{-12} & 1\times10^{-10} & -7\times10^{-13} \end{bmatrix}$$

$$H_i^2 = \begin{bmatrix} 5\times10^{-8} & 3\times10^{-8} & 4\times10^{-8} & -4\times10^{-9} & 3\times10^{-6} & -2\times10^{-7} \\ 2\times10^{-12} & 1\times10^{-12} & 2\times10^{-12} & -2\times10^{-13} & 1\times10^{-10} & 5\times10^{-7} \\ 1\times10^{-12} & 7\times10^{13} & 9\times10^{-13} & -9\times10^{14} & 6\times10^{-11} & 2\times10^{-7} \\ -3\times10^{-12} & -2\times10^{-12} & -2\times10^{-12} & 3\times10^{-13} & -2\times10^{-10} & -9\times10^{-7} \\ 1\times10^{-10} & 8\times10^{-11} & 1\times10^{-10} & -1\times10^{-11} & 7\times10^{-9} & -2\times10^{-6} \\ -7\times10^{-12} & -4\times10^{-12} & -5\times10^{-12} & 6\times10^{-13} & -4\times10^{-10} & -1\times10^{-6} \end{bmatrix}$$

$$H_i^3 = \begin{bmatrix} 5\times10^{-8} & 2\times10^{-12} & 1\times10^{-12} & -3\times10^{-12} & 1\times10^{-10} & -7\times10^{-12} \\ 3\times10^{-8} & 1\times10^{-12} & 7\times10^{-13} & -2\times10^{-12} & 8\times10^{-11} & -4\times10^{-12} \\ 4\times10^{-8} & 2\times10^{-12} & 9\times10^{-13} & -2\times10^{-12} & 1\times10^{-10} & -5\times10^{-12} \\ -4\times10^{-9} & -2\times10^{-13} & -9\times10^{14} & 3\times10^{-13} & -1\times10^{-11} & 6\times10^{-13} \\ 3\times10^{-6} & 1\times10^{-10} & 6\times10^{-11} & -2\times10^{-10} & 7\times10^{-9} & -4\times10^{-10} \\ -2\times10^{-7} & 6\times10^{-7} & 2\times10^{-7} & -9\times10^{-7} & -2\times10^{-6} & -1\times10^{-6} \end{bmatrix}$$

$$H_i^4 = \begin{bmatrix} -8\times10^{-2} & -2\times10^{-5} & -2\times10^{-5} & 2\times10^{-6} & -1\times10^{-3} & 9\times10^{-5} \\ -2\times10^{-5} & -8\times10^{-2} & -1\times10^{-5} & 1\times10^{-6} & -1\times10^{-3} & 6\times10^{-5} \\ -2\times10^{-5} & -2\times10^{-5} & -8\times10^{-2} & 2\times10^{-6} & -1\times10^{-3} & 7\times10^{-5} \\ 2\times10^{-6} & 1\times10^{-6} & 2\times10^{-6} & -8\times10^{-2} & -1\times10^{-4} & -8\times10^{-6} \\ -5\times10^{-4} & -1\times10^{-3} & -1\times10^{-3} & -1\times10^{-4} & -0.1674 & 5\times10^{-3} \\ 9\times10^{-5} & 6\times10^{-5} & 7\times10^{-5} & -8\times10^{-8} & -5\times10^{-3} & -8\times10^{-2} \end{bmatrix}$$

APPENDIX

The system's matrices in Eq. (7) are dertermined as: as shown in the equation at the bottom of the previous page, and

$$D_i = \begin{bmatrix} -4.8 & 0 & 0 & 0 & 0 & 0 \end{bmatrix}^T$$

The system's transfer matrices in Eq. (18) are dertermined as follows:

$$\bar{A}_i = \begin{bmatrix} I^{1\times 6} & \bar{A}_i^{tr} \\ 0^{11\times 6} & I^{11\times 6} \end{bmatrix}; \bar{C}_i = \begin{bmatrix} 0^{1\times 6} & \bar{C}_i^{tr} \\ 0^{11\times 6} & 0^{11\times 6} \end{bmatrix}; \text{ and}$$

$$\bar{D}_i = \begin{bmatrix} \bar{D}_i^{tr} \\ 0^{11\times 6} \end{bmatrix}$$

where:

$$\bar{A}_i^{tr} = \begin{bmatrix} -5.22 & -3.38 & -4.16 & 0.42 & -279.2 & -17.17 \end{bmatrix} \times 10^2$$
$$\bar{C}_i^{tr} = \begin{bmatrix} 0 & 0 & 0 & 0 & 0 & 0.0378 \end{bmatrix};$$

and

$$\bar{D}_i^{tr} = \begin{bmatrix} 0.14 & 0.09 & 0.11 & 0.01 & 7.62 & -0.47 \end{bmatrix}$$

By solving LMI presented in Eq. (19), the following results are obtained:

$$H_i = \begin{bmatrix} H_i^1 & H_i^2 \\ H_i^3 & H_i^4 \end{bmatrix} > 0$$

is a positive definite matrix where, as shown in the equation at the bottom of the previous page.

Thus, the LMI presented in Eq. (19) is feasible.

REFERENCES

[1] U. Akram, M. Nadarajah, R. Shah, and F. Milano, "A review on rapid responsive energy storage technologies for frequency regulation in modern power systems," *Renew. Sustain. Energy Rev.*, vol. 120, Mar. 2020, Art. no. 109626.

[2] H. H. Alhelou, M.-E. Hamedani-Golshan, R. Zamani, E. Heydarian-Forushani, and P. Siano, "Challenges and opportunities of load frequency control in conventional, modern and future smart power systems: A comprehensive review," *Energies*, vol. 11, no. 10, p. 2497, Sep. 2018.

[3] A. Fernández-Guillamón, E. Gómez-Lázaro, E. Muljadi, and Á. Molina-García, "Power systems with high renewable energy sources: A review of inertia and frequency control strategies over time," *Renew. Sustain. Energy Rev.*, vol. 115, Nov. 2019, Art. no. 109369.

[4] Z. Wu, W. Gao, T. Gao, W. Yan, H. Zhang, S. Yan, and X. Wang, "State-of-the-art review on frequency response of wind power plants in power systems," *J. Modern Power Syst. Clean Energy*, vol. 6, no. 1, pp. 1–16, Jan. 2018.

[5] Q. Wang, S. Huang, L. Xiong, Y. Zhou, T. Niu, F. Gao, M. W. Khan, Z. Wang, C. Ban, and R. Song, "Distributed secondary control based on bi-limit homogeneity for AC microgrids subjected to non-uniform delays and actuator saturations," *IEEE Trans. Power Syst.*, vol. 40, no. 1, pp. 820–833, Jan. 2025.

[6] E. Çam, "Application of fuzzy logic for load frequency control of hydroelectrical power plants," *Energy Convers. Manage.*, vol. 48, no. 4, pp. 1281–1288, Apr. 2007.

[7] S. Sondhi and Y. V. Hote, "Fractional order PID controller for load frequency control," *Energy Convers. Manage.*, vol. 85, pp. 343–353, Sep. 2014.

[8] A. Kumar and S. Pan, "Design of fractional order PID controller for load frequency control system with communication delay," *ISA Trans.*, vol. 129, pp. 138–149, Oct. 2022.

[9] Y. V. Hote and S. Jain, "PID controller design for load frequency control: Past, present and future challenges," *IFAC-PapersOnLine*, vol. 51, no. 4, pp. 604–609, 2018.

[10] R. Singh and L. Ramesh, "Comparison between PID and PSO-PID controllers in analysing the load frequency control in interconnected microgrids in a deregulated environment," *Int. J. Global Energy Issues*, vol. 46, nos. 1–2, pp. 112–136, 2024.

[11] M. A. Metwally, M. A. Ali, S. A. Kutb, and F. M. Bendary, "A genetic algorithm for optimum design of PID controller in multi area load frequency control for Egyptian electrical grid," *Int. J. Eng. Res. Technol.*, vol. 5, no. 10, pp. 1–9, 2024.

[12] I. F. Davoudkhani, P. Zare, S. J. S. Shenava, A. Y. Abdelaziz, M. Bajaj, and M. B. Tuka, "Maiden application of mountaineering team-based optimization algorithm optimized 1PD-PI controller for load frequency control in islanded microgrid with renewable energy sources," *Sci. Rep.*, vol. 14, no. 1, Oct. 2024, Art. no. 22851.

[13] A. Tabak and S. Duman, "Maiden application of TIDμ1NDμ2 controller for effective load frequency control of non-linear two-area power system," *IET Renew. Power Gener.*, vol. 18, no. 7, pp. 1269–1291, May 2024.

[14] I. F. Davoudkhani, P. Zare, A. Y. Abdelaziz, M. Bajaj, and M. B. Tuka, "Robust load-frequency control of islanded urban microgrid using 1PD-3DOF-PID controller including mobile EV energy storage," *Sci. Rep.*, vol. 14, no. 1, Jun. 2024, Art. no. 13962.

[15] H. Shayeghi, I. F. Davoudkhani, and N. Bizon, "Robust self-adaptive fuzzy controller for load-frequency control of islanded airport microgrids considering electric aircraft energy storage and demand response," *IET Renew. Power Gener.*, vol. 18, no. 4, pp. 616–653, Mar. 2024.

[16] R. Kumar and A. Sikander, "A new hybrid approach based on fuzzy logic and optimization for load frequency control," *Int. J. Model. Simulation*, pp. 1–10, Feb. 2024, doi: 10.1080/02286203.2024.2315327.

[17] P. C. Nayak, R. C. Prusty, and S. Panda, "Adaptive fuzzy approach for load frequency control using hybrid moth flame pattern search optimization with real time validation," *Evol. Intell.*, vol. 17, no. 2, pp. 1111–1126, Apr. 2024.

[18] Z. Yan and Y. Xu, "A multi-agent deep reinforcement learning method for cooperative load frequency control of a multi-area power system," *IEEE Trans. Power Syst.*, vol. 35, no. 6, pp. 4599–4608, Nov. 2020.

[19] J. Li, T. Yu, and X. Zhang, "Coordinated load frequency control of multi-area integrated energy system using multi-agent deep reinforcement learning," *Appl. Energy*, vol. 306, Jan. 2022, Art. no. 117900.

[20] Y. Zhang, X. Shi, H. Zhang, Y. Cao, and V. Terzija, "Review on deep learning applications in frequency analysis and control of modern power system," *Int. J. Electr. Power Energy Syst.*, vol. 136, Mar. 2022, Art. no. 107744.

[21] K. P. S. Parmar, S. Majhi, and D. P. Kothari, "Load frequency control of a realistic power system with multi-source power generation," *Int. J. Electr. Power Energy Syst.*, vol. 42, no. 1, pp. 426–433, Nov. 2012.

[22] C. Lin, B. Hu, C. Shao, W. Li, C. Li, and K. Xie, "Delay-dependent optimal load frequency control for sampling systems with demand response," *IEEE Trans. Power Syst.*, vol. 37, no. 6, pp. 4310–4324, Nov. 2022.

[23] M. M. Gulzar, D. Sibtain, A. Ahmad, I. Javed, S. Murawwat, I. Rasool, and A. Hayat, "An efficient design of adaptive model predictive controller for load frequency control in hybrid power system," *Int. Trans. Electr. Energy Syst.*, vol. 2022, Apr. 2022, Art. no. 7894264.

[24] H. H. Ali, A. M. Kassem, M. Al-Dhaifallah, and A. Fathy, "Multi-verse optimizer for model predictive load frequency control of hybrid multi-interconnected plants comprising renewable energy," *IEEE Access*, vol. 8, pp. 114623–114642, 2020.

[25] L. Xiong, R. Song, S. Huang, C. Ban, P. Li, Z. Wang, M. W. Khan, and T. Niu, "Markov jump system modeling and control of inverter-fed remote area weak grid via quantized sliding mode," *IEEE Trans. Power Syst.*, early access, Nov. 11, 2024, doi: 10.1109/TPWRS.2024.3494857.

[26] C. Wang, Y. Mi, Y. Fu, and P. Wang, "Frequency control of an isolated micro-grid using double sliding mode controllers and disturbance observer," *IEEE Trans. Smart Grid*, vol. 9, no. 2, pp. 923–930, Mar. 2018.

[27] S. Prasad, S. Purwar, and N. Kishor, "Non-linear sliding mode load frequency control in multi-area power system," *Control Eng. Pract.*, vol. 61, pp. 81–92, Apr. 2017.

[28] J. Guo, "Application of full order sliding mode control based on different areas power system with load frequency control," *ISA Trans.*, vol. 92, pp. 23–34, Sep. 2019.

[29] A. Bagheri, A. Jabbari, and S. Mobayen, "An intelligent ABC-based terminal sliding mode controller for load-frequency control of islanded micro-grids," *Sustain. Cities Soc.*, vol. 64, Jan. 2021, Art. no. 102544.

[30] K. Vrdoljak, N. Perić, and I. Petrović, "Sliding mode based load-frequency control in power systems," *Electric Power Syst. Res.*, vol. 80, no. 5, pp. 514–527, May 2010.
[31] J. Ansari, M. Homayounzade, and A. R. Abbasi, "Load frequency control in power systems by a robust backstepping sliding mode controller design," *Energy Rep.*, vol. 10, pp. 1287–1298, Nov. 2023.
[32] Y. Mi, Y. Fu, C. Wang, and P. Wang, "Decentralized sliding mode load frequency control for multi-area power systems," *IEEE Trans. Power Syst.*, vol. 28, no. 4, pp. 4301–4309, Nov. 2013.
[33] A.-T. Tran, N. T. Pham, V. Van Huynh, and D. N. M. Dang, "Stabilizing and enhancing frequency control of power system using decentralized observer-based sliding mode control," *J. Control, Autom. Electr. Syst.*, vol. 34, no. 3, pp. 541–553, Jun. 2023.
[34] V. Patel, V. K. Giri, and A. Kumar, "Fractional-order adaptive sliding mode control with disturbance observer for frequency regulation in isolated microgrid," *Int. J. Dyn. Control*, vol. 12, no. 6, pp. 2010–2019, Jun. 2024.
[35] A.-T. Tran, B. Le Ngoc Minh, P. T. Tran, V. V. Huynh, V.-D. Phan, V.-T. Pham, and T. M. Nguyen, "Adaptive integral second-order sliding mode control design for load frequency control of large-scale power system with communication delays," *Complexity*, vol. 2021, no. 1, Jan. 2021, Art. no. 5564184.
[36] A. Tran, M. P. Duong, N. T. Pham, and J. W. Shim, "Enhanced sliding mode controller design via meta-heuristic algorithm for robust and stable load frequency control in multi-area power systems," *IET Gener., Transmiss. Distrib.*, vol. 18, no. 3, pp. 460–478, Feb. 2024.
[37] J. Guo, "A novel proportional-derivative sliding mode for load frequency control," *IEEE Access*, vol. 12, pp. 127417–127425, 2024.
[38] W.-S. Lin and C.-S. Chen, "Robust adaptive sliding mode control using fuzzy modelling for a class of uncertain MIMO nonlinear systems," *IEE Proc.-Control Theory Appl.*, vol. 149, no. 3, pp. 193–202, May 2002.
[39] D. W. C. Ho and Y. Niu, "Robust fuzzy design for nonlinear uncertain stochastic systems via sliding-mode control," *IEEE Trans. Fuzzy Syst.*, vol. 15, no. 3, pp. 350–358, Jun. 2007.
[40] K. P. S. Parmar, S. Majhi, and D. P. Kothari, "LFC of an interconnected power system with multi-source power generation in deregulated power environment," *Int. J. Electr. Power Energy Syst.*, vol. 57, pp. 277–286, May 2014.
[41] V. V. Huynh, P. T. Tran, T. M. Nguyen, V.-D. Phan, and V.-T. Pham, "Advanced sliding mode observer design for load frequency control of multiarea multisource power systems," *Int. Trans. Electr. Energy Syst.*, vol. 2022, Mar. 2022, Art. no. 6587194.
[42] X. Chen, M. Zhang, Z. Wu, L. Wu, and X. Guan, "Model-free load frequency control of nonlinear power systems based on deep reinforcement learning," *IEEE Trans. Ind. Informat.*, vol. 20, no. 4, pp. 6825–6833, Apr. 2024.

DAO TRONG TRAN was born in Vietnam. He received the B.Eng. and M.Eng. degrees in automatic control and engineering informatics from the VSB-Technical University of Ostrava, in 2004 and 2006, respectively, and the Ph.D. degree in technical cybernetics from Tomas Bata University in Zlin, in 2009. He went to the VSB-Technical University of Ostrava, in 2001. He is currently a Researcher and an University Lecturer with the Faculty of Information Technology, Ton Duc Thang University. He has co-authored research papers and articles in international journals, conference proceedings, conference paper presentations, and book chapters; and an Editor of *AETA Proceedings: Recent Advances in Electrical Engineering and Related Sciences*. His research interests include the fields of applied informatics and control, modeling and simulation systems, optimization systems, artificial intelligence and application, and evolutionary algorithms. He is also a member of MERLIN and NAVY Research Groups.

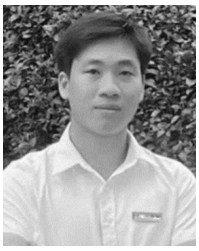

ANH-TUAN TRAN received the B.Eng. degree in electrical and electronics engineering and the M.Eng. degree in electrical engineering from Ton Duc Thang University (TDTU), Ho Chi Minh City, Vietnam, in 2019 and 2021, respectively. He is currently a member of the Modeling Evolutionary Algorithms Simulation and Artificial Intelligence Research Group, Faculty of Electrical and Electronics Engineering, Ton Duc Thang University. His research interests include power system dynamics, stability and control, energy storage systems, sliding mode control, optimal control, observer, and optimization algorithms.

VAN VAN HUYNH received the Ph.D. degree in mechanical and automation control engineering from Da-Yeh University, Taiwan, in 2015. He is currently a Lecturer with the Faculty of Electrical and Electronics Engineering, Ton Duc Thang University, Ho Chi Minh City, Vietnam. His research interests include sliding mode control, variable structure control, and power system control.

TON DUC DO (Senior Member, IEEE) received the B.S. and M.S. degrees in electrical engineering from Hanoi University of Science and Technology, Hanoi, Vietnam, in 2007 and 2009, respectively, and the Ph.D. degree in electrical engineering from Dongguk University, Seoul, South Korea, in 2014.

From 2008 to 2009, he was with the Division of Electrical Engineering, Thuy Loi University, Vietnam, as a Lecturer. He was a Postdoctoral Researcher with the Division of Electronics and Electrical Engineering, Dongguk University, in 2014. He was also a Senior Researcher with the Pioneer Research Center for Controlling Dementia by Converging Technology, Gyeongsang National University, South Korea, from May 2014 to August 2015. Since September 2015, he has been an Assistant Professor and promoted to an Associate Professor with the Department of Robotics and Mechatronics, Nazarbayev University, Kazakhstan. His research interests include the field of control engineering, electric drives, renewable energy conversion systems, and nanorobots. He was an Associate Editor of IEEE Access, from April 2017 to August 2024, and IEEE Robotics and Automation Letters, since August 2023. He has been promoted to be a Senior Editor of IEEE Access, since May 2024. He has also been a Guest Editor of special issues of several journals, such as *Mathematical Problems in Engineering*, *Electronics*, *Energies*, *Sensors*, *Fractals and Fractional*, and *International Journal of Advanced Robotic Systems*. He received the Best Research Award from Dongguk University, in 2014, the Most Cited Paper Award from Wind Energy, in 2020 and 2021, and the Outstanding Associate Editor Award of IEEE Access, in 2021, 2022, and 2023. He has been listed in the top 2% of scientists based on the citation on the single-year table, since 2019, and career-wide table, since 2021. He received the Medal from the Minister of Science and Education for outstanding contribution to science in Kazakhstan, in 2024.